Constitutive relationship and kinetics model of DRX during thermal deformation of Stellite 6B alloy

Zhang Yawei [a,b], Zhang Shixiao [b], Lu Xudong [a,b,*]

[a]Beijing Key Laboratory of Advanced High Temperature Materials, Central Iron and Steel Research Institute, Beijing 100081, China

[b]Beijing Gaona Aero Material CO., LTD., Beijing 100081, China

*Corresponding author. Tel.: +86-10-62186190. E-mail address: lxdong0700@hotmail.com

Abstract

Stellite 6B superalloy is widely used in the harsh industrial environment, because of excellent wear characteristics, hot hardness, good corrosion resistance, and superior mechanical properties. Hot compression tests were performed on Stellite 6B alloy to study high temperature dynamic recrystallization behavior during thermal deformation. The tests were performed in the temperature 1000 °C, 1050 °C, 1100 °C, 1150 °C and 1200 °C and at the strain rates of 0.01 s^{-1}, 0.1 s^{-1}, 1 s^{-1} and 10 s^{-1}. Stress-strain curves, constitutive relationship, and the DRX model of the Stellite 6B alloy were investigated. The results showed that the dynamic recrystallization was easily beginning, the dynamic recovery process is inhibited, and the softening effect by dynamic recrystallization is more significant.

Keywords: Stellite 6B alloy; Dynamic recrystallization; Kinetics model; Microstructure; Thermal deformation.

Introduction

Stellite 6B is a typical carbide-hardened Co-based wear-resistant superalloy, and it has been widely used in rock crushing rollers, cement and steel equipment, transmission devices, and other industrial fields, especially in sleeves that cannot be fully lubricated [1], because of their inherent high-strength, corrosion resistance and ability to retain hardness at elevated temperatures [2, 3]. The typical microstructure of such alloys consists of hard carbides dispersed in a cobalt-rich solid solution matrix. The Co-based alloy has a relatively low stacking fault energy, which is easily transformed from metastable FCC structure to a stable HCP structure during the process of processing or service [1]. The presence and distribution of hard phases have already been identified as the main factor responsible for the enhanced high temperature resistance (up to 600 °C) to sliding wear [1, 4-8].

Comparing to much harder cast Co-based alloy, the wrought structure has excellent abrasion wear resistance. Dynamic recrystallization (DRX) is considered as one of the most important microstructural evolution mechanisms, which is beneficial to obtain fine metallurgical structures, eliminate defects and improve mechanical properties of products [9-14]. A. Gholipour [15] investigated the influence of microstructure on the wear properties of Stellite 6. The effect of molybdenum on the microstructure and the tribological properties of the Stellite alloys were also investigated [2, 16-18]. However, there are still only a few reports in the literature so far concerning the dynamic recrystallization behavior and microstructure evolution of Stellite 6B alloy during thermal deformation. In this paper, hot compression tests were performed on Stellite 6B alloy to study high temperature dynamic recrystallization behavior. The thermal deformation constitutive relationship model, and the dynamic recrystallization kinetics equation of the alloy was established.

Experimental procedures

The chemical compositions (wt.%) of Stellite 6B used in this investigation are as follows: C 1.2; Cr 30; Mo 1.2; W 4.5; Ni 2.0; Si 1.0; Mn 1.0; Fe<3.0; Co balance. Several 12.5mm thick sheets was cut from an as-received wrought bar (40 mm in diameter) in the direction of cross section. Cylindrical specimens, with a diameter of 8 mm and a height of 12 mm, were machined from the center part to ensure the uniformity of microstructure for all the specimens. The specimens were then solution treated at 1220 °C for 30 min before compression tests.

The isothermal compression tests were performed on the thermomechanical simulator

Gleeble-3800 at the temperatures ranging from 1000 °C to 1200 °C at the intervals of 50 °C and at the strain rates of 0.01 s^{-1}, 0.1 s^{-1}, 1 s^{-1} and 10 s^{-1}.

Results and discussion

True stress-true stain curves

Fig. 1 shows the true stress-true strain curves of Stellite 6B alloy obtained under different temperatures and strain rates. The flow stress curves exhibit the similar features, i.e. a single peak near the critical strain followed by a strain softening stage and then sometimes a steady stage at high strain zone. The characteristics of the flow stress curves are the typical ones observed in low stacking-fault energy alloy, which implies the happening of DRX phenomenon during thermal deformation[9]. In the initial stage of the forming process, the flow stress abruptly increases due to the dominance of work hardening, because of that the softening effect caused by dynamic recovery is not sufficient to offset the work hardening. When deformation exceeds the peak strain, the flow stress decreases with increasing stain as softening caused by DRX overtakes hardening caused by work hardening. Then the flow stress shows steady state region due to the equilibrium of dynamic softening and work hardening.

The flow stresses are dependent on the deformation variables, such as temperature, strain rate and strain. As temperature decreases at the constant strain rate, the overall level of the flow curve enhances correspondingly due to the decreasing in the dislocation slip and the diffusion ability of grain boundaries for the annihilation of dislocations. Meanwhile, the flow stress increases with the increasing strain rate at the constant deformation temperature. This is mainly due to the fact that the lower strain rate provides the longer time for dislocation annihilation and then reduces the flow stress.
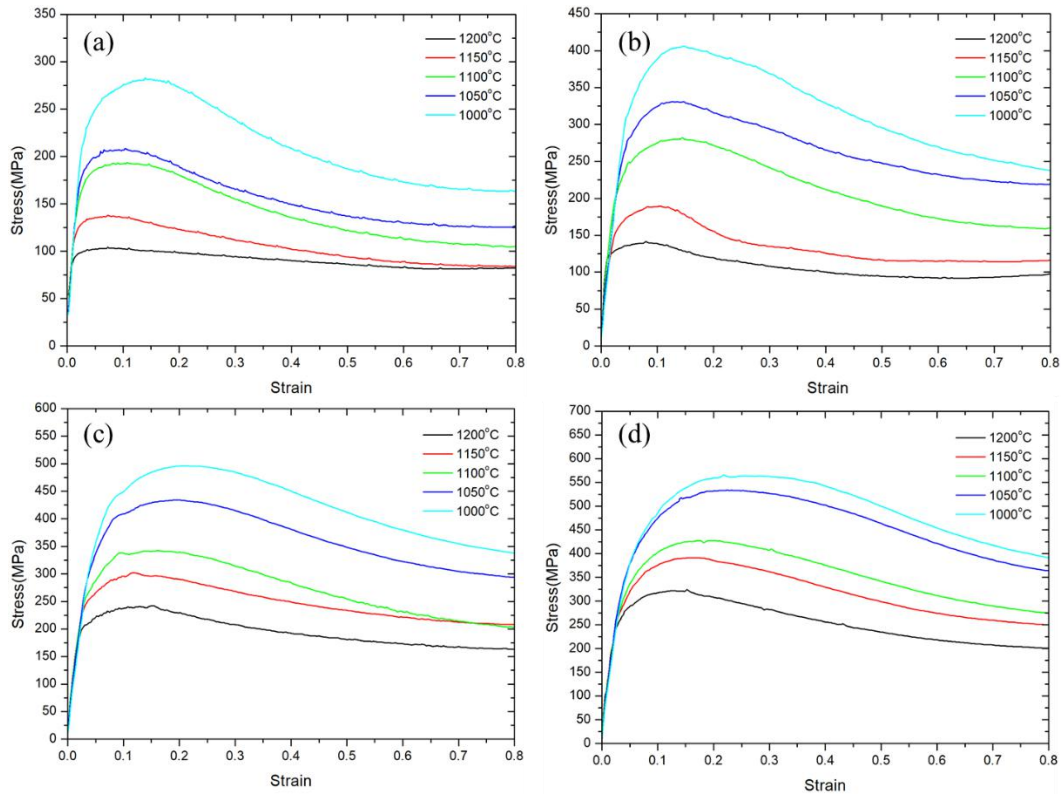
Fig.1. Flow stress curves of Stellite 6B alloy at different temperatures and strain rates of

(a) 0.01s⁻¹, (b) 0.1 s⁻¹, (c) 1 s⁻¹, (d) 10 s⁻¹.

Peak stress is an important indicator in the process of thermal processing, which determines the setting of the power parameters and the microstructure evolution. The peak stress of Stellite 6B alloy in different deformation temperature and strain rate is shown in fig. 2, and it can be observed that the peak stress decreases with the decreasing strain rates and the increasing temperature, which is a conventional behavior and consistent with other reports for superalloys [19-21]. It is worth mentioning that the peak strain (the one associated to the peak stress), which is usually associated to the onset of DRX, is also decreases with decreasing strain rates and the increasing temperature.
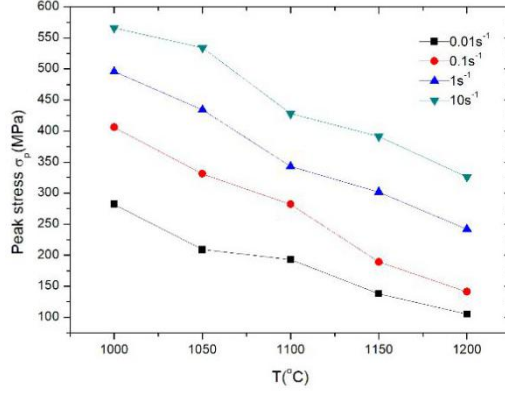
4

Fig. 2. Schematic of the dependence of peak stress σ_p on strain rates and temperatures.

Constitutive relationship

Several researchers in the past have developed different constitutive models for modeling the flow behavior. Sellers model，which is used in this paper，is a phenomenological model that has been extensively used for determining the constitutive relationship in superalloys. The Zener-Hollomon parameter is defined as:

$$Z = \dot{\varepsilon}exp\left[Q/(RT)\right] \qquad (1)$$

where, $\dot{\varepsilon}$ is the strain rate, Q is the effective activation energy for deformation, R is the gas constant and T is the temperature.

Sellars and Whiteman pointed out that the stress can be considered to be dependent on the temperature and strain rate and modeled using creep equation for high and low stress level [22]:

$$Z = A[sinh\,(\alpha\sigma)]^n \qquad (2)$$

where $\alpha=\beta/n$，n，β，A are the undetermined parameters; A is a structure factor, s^{-1}; α is stress multiplier, MPa^{-1}; n is stress exponent.

McQueen et al.[23] have pointed out that for metal with DRX, σ can be referred to the peak stress σ_p. The approximate value of n can be taken as the slope of the plot of $ln\dot{\varepsilon}$ versus $ln\sigma_p$ at the low stress level. The value of A and β can be determined according to the $ln\dot{\varepsilon}$ versus σ_p plot at the high stress level. The first term represents the slope of the $ln\,(sin\,h\,(\alpha\sigma_p))$ versus $1/T$ plot and the second term represents the reciprocal value of inclination of the $ln\,(sin\,h\,(\alpha\sigma_p))$ versus $ln\dot{\varepsilon}$ plot. The approximate value of n is 7.4313 according to Fig. 3(a), and that of β is 0.02604 according to Fig. 3(b). So, the suitable value of α is 0.003504. According to Fig. 3(c) and (d), the value of Q equals 479.997 kJ/mol. Then, the value of A can be calculated

as $1.87 \times 10^{14} s^{-1}$ and the corresponding Z parameter and the constitutive relationship can be obtained:

$$Z = \dot{\varepsilon} exp(479997/(RT))) \tag{3}$$

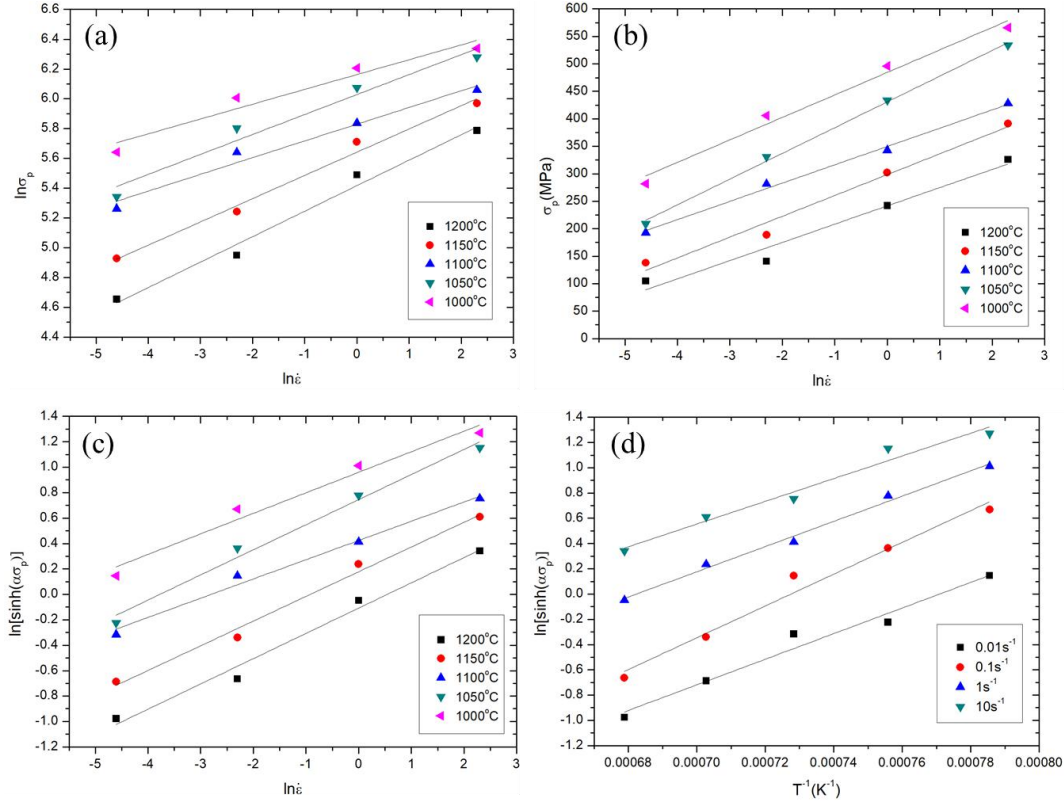$$\dot{\varepsilon} = 1.87 \times 10^{14}[sinh(0.003504\sigma)]^{7.4313} exp(-479997/(RT))) \tag{4}$$

Fig. 3. Schematic of the dependence of the peak stress on temperature and strain rate: (a) Schematic of $ln\sigma_p$ versus $ln\dot{\varepsilon}$, (b) Schematic of σ_p versus $ln\dot{\varepsilon}$, (c) schematic of $ln(sin\ h\ (\alpha\sigma p))$ versus $ln\dot{\varepsilon}$, (d) schematic of $ln(sin\ h\ (\alpha\sigma p))$ versus $1/T$.

Processing map

The processing map can be a suitable approach to establish a relation between the material constitutive behavior and its microstructure evolution, flow instability and hot workability [24, 25]. Fig. 4 shows the processing map of the test alloy Stellite 6B at the strain of 0.3 and 0.5.

The shaded areas in the processing map indicate that when the strain rate exceeds $1s^{-1}$, the flow instability will occur at low or high testing temperatures. The deformation of the material in the regime was reported to be inhomogeneous and adiabatic shear bands were produced in the microstructure [24]. When the specimen was deformed at high strain rates ($>1s^{-1}$), the heat generated by deformation is not conducted away since the thermal conductivity is low and the time available is too short. So, the temperature rises and leads to a decrease of the strength,

and further deformation is preferred in the hot softening area thereby causing localization. The maps obtained at strains of 0.5 are essentially similar to that obtained at a strain of 0.3, which indicates that strain does not have a significant influence [26].

It can be evidently observed that the efficiency of power dissipation η-value declined rapidly is situated in the low temperature high strain rate region and high temperature low strain rate region. Apparently, it is related to the incompatible deformation at the low temperature high strain rate and the coarse grain at the high temperature low strain rate [19, 26, 27].
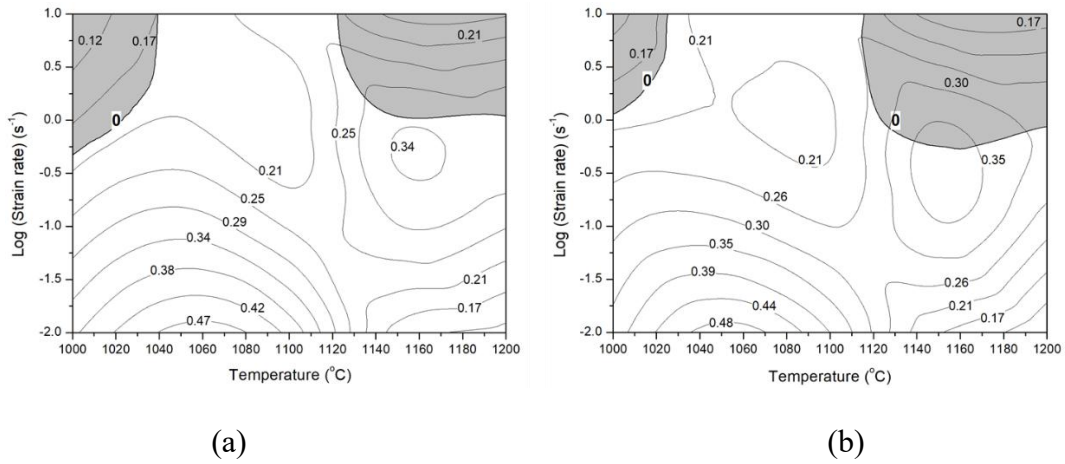

(a)   (b)

Fig. 4. Processing map for Stellite 6B at strain of (a) 0.3 (b) 0.5

Critical strain of DRX

Critical strain ε_c, which represents the initiating dynamic recrystallization, is one of the important parameters of the dynamic recrystallization. DRX is initiated at the critical strain ε_c and critical stress σ_c, after which it leads to more and more softening. The accurate description of the influence of deformation conditions on critical strain is the key to the DRX kinetics model. It is difficult to determine the critical strain of the alloy dynamic recrystallization through the metallographic organization, which requires a large analysis of the microstructural evolution during the dynamic recrystallization.

According to Poliak and Jonas[9], DRX leads to the appearance of a point of inflection in the strain hardening rate θ $(\theta=d\sigma/d\varepsilon)$ vs σ curve, at which $d^2\theta/d^2\sigma=0$ or $d^2\theta/d^2\sigma$ showed a sharp decline. The turning point of $ln\theta$-ε curve also can be observed, for the relation $d(ln\theta)/d\varepsilon=-d\theta/d\sigma$ can be derived by using partial derivatives. For Stellite 6B alloy with low stacking-fault energy, it is not easy for the dislocation to slip at the initial stage of deformation, and the work hardening rate increases rapidly until dynamic recrystallization begins. The relative change from the critical stress to the peak stress is small, while the relative change

from the critical strain to the peak strain is large. Therefore, it is more accurate to confirm the critical stain by determining the position of the inflection point of $ln\theta$-ε curve. Based on the above theoretical derivation, the critical strain value ε_c can be obtained by using the relationship between $ln\theta$ and ε.
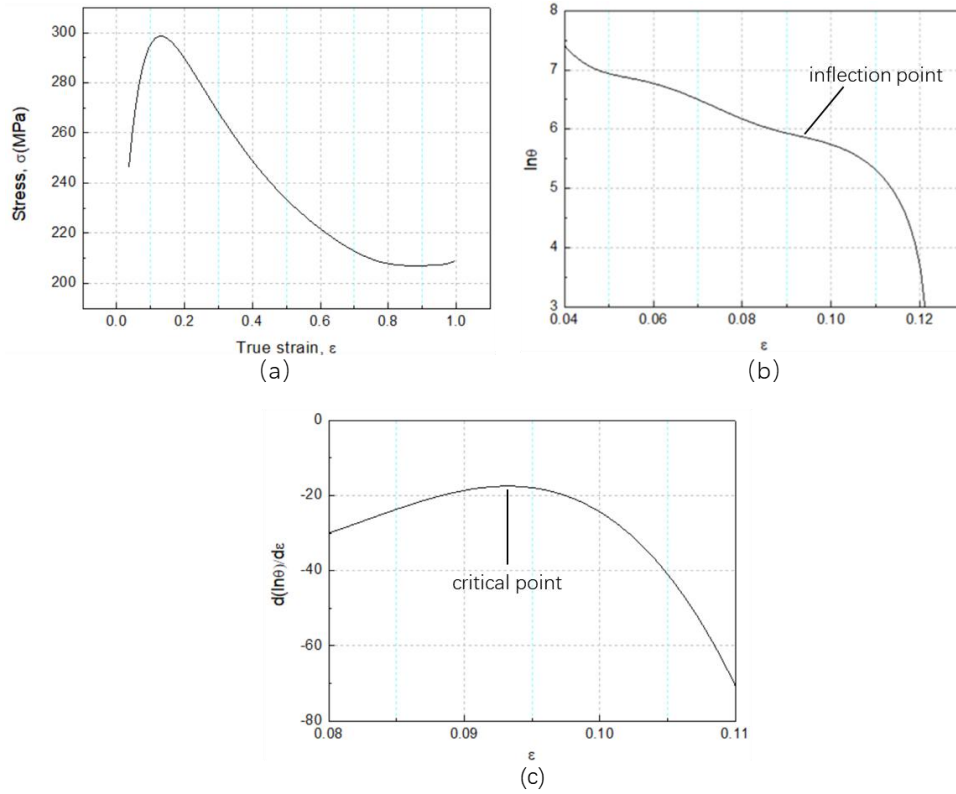

Fig.5. Schematic of the relationship between strain hardening rate and strain at the temperature of 1150°C and the strain rate of 1 s⁻¹ for Stellite 6B (a) σ vs. ε (b) $ln\theta$ vs. ε (c) $d(ln\theta)/d\varepsilon$ vs. ε

Taking the stress-strain curve at the temperature of 1150 °C and the strain rate of 1 s⁻¹ as an example, the relationship between σ and ε, which is obtained by seventh-order polynomial fitting, the relationship between $ln\theta$ and ε and the relationship between $d(ln\theta)/d\varepsilon$ and ε are shown in Fig. 5(a)–(c), respectively. The inflection point appears near the true strain 0.09 on the $ln\theta$-ε curve, as showed in Fig. 5 (b). In order to determine the specific position of the inflection point, $d(ln\theta)/d\varepsilon$-ε curve are plotted by taking the derivative of the $ln\theta$-ε curve after polynomial fitting, as shown in Fig. 5 (c), and it can be found that $d(ln\theta)/d\varepsilon$ increases to a peak value, that corresponding to the critical strain ε_c =0.093. The above methods can be used to determine the critical strain under each deformation condition, as shown in Table 1. It can be seen that the critical strain increases with increasing of strain rate and decreasing of deformation temperature, and under all deformation conditions, dynamic recrystallization begins when the true strain is less than 0.16. Because of the low stacking-fault energy of

Co-rich matrix, the energy can be accumulated quickly to reach the condition of recrystallization nucleation. In addition, it is conducive to the formation of recrystallize core that the dislocations piled up on the interface of the hard-deformable carbides with a volume fraction of more than 20%.

Table 1   The values of the ε_c under each strain rates and temperatures.

Strain rate	Temperature				
	1000°C	1050°C	1100°C	1150°C	1200°C
0.01s⁻¹	0.09	0.05	0.06	0.05	0.06
0.1s⁻¹	0.09	0.09	0.08	0.06	0.06
1s⁻¹	0.13	0.14	0.10	0.09	0.08
10s⁻¹	0.15	0.16	0.14	0.12	0.11

The relationship of $ln\varepsilon_c$ and lnZ is approximate linear and linear regression equation obtained according to Fig. 6 is as follows:

$$ln\varepsilon_c = 0.10001lnZ - 6.51796 \qquad (5)$$

Therefore, the relationship between the critical strain ε_c and Z parameters can be expressed as follows:

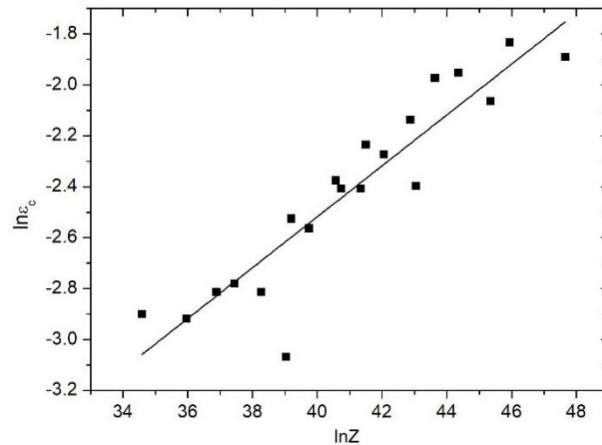$$\varepsilon_c = 0.001477Z^{0.10001} \qquad (6)$$

Fig. 6. Schematic of the dependence of ε_c on Z parameter

Kinetics model of DRX

Due to the great impact of DRX on hot working flow stress and its effect on the microstructure and properties of the materials after processing, the prediction of DRX kinetics

9

is of considerable importance in the modeling of industrial hot working processes. According to the classic theory, the development process of DRX is similar to that of phase transition. The velocity of DRX begins from zero and slowly increases, and after a latent period the velocity of DRX starts to rapidly increase, and after it reaches the maximum the velocity of DRX gradually decreases, in the end the velocity of DRX is close to zero.

Generally, JMAK model is used to describe the DRX kinetics dynamic recrystallization of alloys, that is, the DRX volume fraction is expressed as a function of deformation time as follows:

$$X_{DRX} = 1 - \exp\left[-0.693\left(\frac{t}{t_{0.5}}\right)^k\right] \tag{7}$$

where X_{DRX} is the dynamically recrystallized volume fraction, $t_{0.5}$ is the time for 50% DRX, t is the time for X_{DRX} to occur. In this model, the using of the constant 0.693 is crucial and very skillful, which make all the parameters have obvious physical meanings. But a lot of works needs to do to calculate the recrystallization fraction of the alloy after rapid cooling under different deformation conditions at multiple time intervals.

Kim and co-workers[10, 13], developed the following DRX kinetics model in the form of modified Avrami equation based on the thermomechanical simulation tests, the equation is as follows:

$$\begin{cases} X_{DRX} = 1 - exp\left[-\left(\frac{\varepsilon - \varepsilon_c}{\varepsilon^*}\right)^m\right] \\ m = 1.12\left(\frac{Z}{A}\right)^{-0.08} \end{cases} \tag{8}$$

where ε^* is the strain for maximum softening rate, i.e. the minimum value of θ-ε curve.

It can be seen from Fig. 7 that the work hardening rates of the alloy under all conditions decrease rapidly to the minimum value, which ate corresponding to the maximum softening rate strains, and then increase faster than usual superalloys. As shown in Table 2, the maximum softening rate strain ε^* increases with increasing strain rate and decreasing temperature, that is, higher temperature and lower rolling speed are beneficial to the deformation of the alloy.
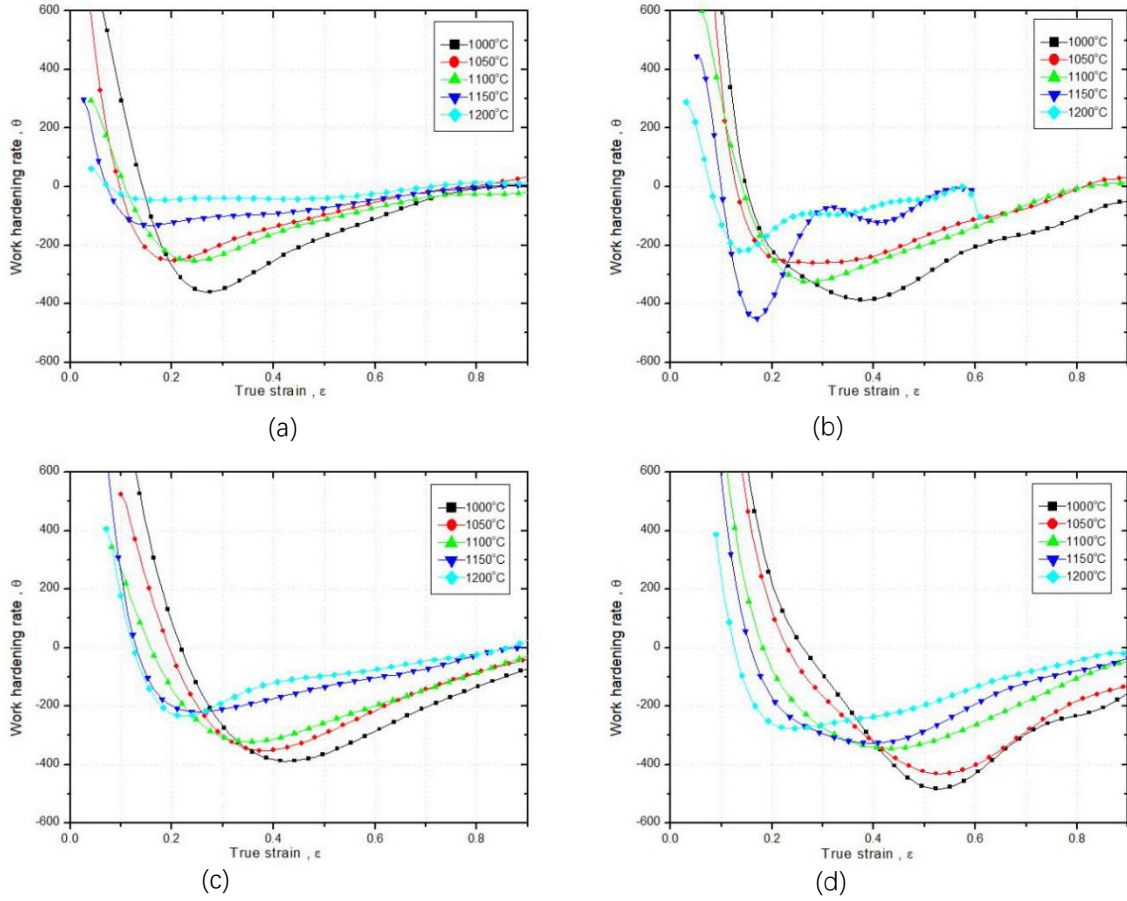
Fig. 7 Schematic of the relationship between θ and ε for Stellite 6B alloy

（a）0.01s⁻¹，（b）0.1s⁻¹，（c）1s⁻¹，（d）10s⁻¹

Table 2   The values of the ε^* under each strain rates and temperatures.

Strain rate	Temperature				
	1000°C	1050°C	1100°C	1150°C	1200°C
0.01s⁻¹	0.27	0.2	0.24	0.156	0.17
0.1s⁻¹	0.38	0.29	0.28	0.17	0.143
1s⁻¹	0.42	0.38	0.35	0.25	0.23
10s⁻¹	0.52	0.53	0.43	0.4	0.24

The relationship of $ln\varepsilon^*$ and lnZ is approximate linear and linear regression equation obtained according to Fig. 8 is as follows:

$$ln\varepsilon^* = 0.10834 lnZ - 5.71234 \tag{9}$$

Therefore, the relationship between the maximum softening rate strain ε^* and Z parameters can be expressed as follows:

$$\varepsilon^* = 0.003305Z^{0.10834} \tag{10}$$

Finally, the as-obtained DRX kinetic model is described as:

$$\begin{cases} X_{\text{DRX}} = 1 - exp\left[-\left(\frac{\varepsilon-\varepsilon_c}{\varepsilon^*}\right)^m\right] \\ m = 1.12\left(\frac{Z}{A}\right)^{-0.08} \\ \varepsilon_c = 0.001477Z^{0.10001} \\ \varepsilon^* = 0.003305Z^{0.10834} \end{cases} \tag{11}$$
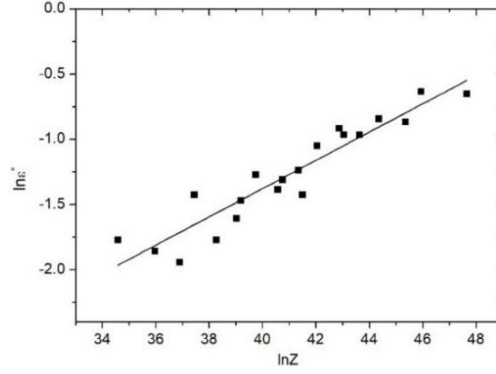

Fig. 8 Schematic of the dependence of ε^* on Z parameter

Conclusions

Hot compression test in the temperature range of 1000-1200 °C, and strain rate range of 0.001-10 s^{-1} of Stellite 6B Co-based alloy has been conducted. The following conclusions can be drawn from of the results of this investigation:

(1) The constitutive relationship of the wrought Stellite 6B alloy could be expressed as:

$$\dot{\varepsilon} = 1.87 \times 10^{14}[sinh(0.003504\sigma)]^{7.4313}exp(-479997/(RT))$$

(2) The following DRX kinetic model can be used to express dynamic recrystallization behavior of the investigated alloy:

$$\begin{cases} X_{\text{DRX}} = 1 - exp\left[-\left(\frac{\varepsilon-\varepsilon_c}{\varepsilon^*}\right)^m\right] \\ m = 1.12\left(\frac{Z}{A}\right)^{-0.08} \\ \varepsilon_c = 0.001477Z^{0.10001} \\ \varepsilon^* = 0.003305Z^{0.10834} \end{cases}$$

References

[1] M.X. Yao, J.B.C. Wu, W. Xu, R. Liu, Metallographic study and wear resistance of a high-C wrought Co-based alloy Stellite 706K, Materials Science and Engineering: A 407(1-2) (2005) 291-298.

[2] U. Malayoglu, A. Neville, Mo and W as alloying elements in Co-based alloys—their effects on erosion–corrosion resistance, Wear 259(1-6) (2005) 219-229.

[3] W.S. da Silva, R.M. Souza, J.D.B. Mello, H. Goldenstein, Room temperature mechanical properties and tribology of NICRALC and Stellite casting alloys, Wear 271(9-10) (2011) 1819-1827.

[4] H. Berns, Microstructural properties of wear-resistant alloys, Wear 181-183 (1995) 271-279.

[5] J.N. Aoh, J.C. Chen, On the wear characteristics of cobalt-based hardfacing layer after thermal fatigue and oxidation, Wear 250 (2001) 611-620.

[6] M. Sebastiani, V. Mangione, D. De Felicis, E. Bemporad, F. Carassiti, Wear mechanisms and in-service surface modifications of a Stellite 6B Co–Cr alloy, Wear 290-291 (2012) 10-17.

[7] P.D. Wood, H.E. Evans, C.B. Ponton, Investigation into the wear behaviour of Stellite 6 during rotation as an unlubricated bearing at 600°C, Tribology International 44(12) (2011) 1589-1597.

[8] W. Gao, Y. Lian, G. Xie, J. Huang, L. Zhang, M. Ma, C. Zhao, Z. Zhang, K. Liu, S. Zhang, J. Zhang, Study of dry sliding wear characteristics of stellite 6B versus AISI M2 steel at various sliding velocities, Wear 402-403 (2018) 169-178.

[9] E.I. Poliak, J.J. Jonas, A one parameter approach to determining the critical conditions for the initiation of dynamic recrystallization, Acta Materialia 44 (1996) 127-136.

[10] S.-I. Kim, Y.-C. Yoo, Dynamic recrystallization behavior of AISI 304 stainless steel, Materials Science and Engineering A 311 (2001) 108-113.

[11] P. Poelt, C. Sommitsch, S. Mitsche, M. Walter, Dynamic recrystallization of Ni-base alloys—Experimental results and comparisons with simulations, Materials Science and Engineering: A 420(1-2) (2006) 306-314.

[12] J. Huang, Z. Xu, Evolution mechanism of grain refinement based on dynamic recrystallization in multiaxially forged austenite, Materials Letters 60(15) (2006) 1854-1858.

[13] S.-I. Kim, Y. Lee, D.-L. Lee, Y.-C. Yoo, Modeling of AGS and recrystallized fraction of microalloyed medium carbon steel during hot deformation, Materials Science and Engineering: A 355(1-2) (2003) 384-393.

[14] Y. Wang, W.Z. Shao, L. Zhen, X.M. Zhang, Microstructure evolution during dynamic recrystallization of hot deformed superalloy 718, Materials Science and Engineering: A 486(1-2) (2008) 321-332.

[15] A. Gholipour, M. Shamanian, F. Ashrafizadeh, Microstructure and wear behavior of stellite 6 cladding on 17-4 PH stainless steel, Journal of Alloys and Compounds 509(14) (2011) 4905-4909.

[16] J.-C. Shin, J.-M. Doh, J.-K. Yoon, D.-Y. Lee, J.-S. Kim, Effect of molybdenum on the microstructure and wear resistance of cobalt-base Stellite hardfacing alloys, Surface and Coatings Technology 166 (2003) 117-126.

[17] P. Huang, R. Liu, X. Wu, M.X. Yao, Effects of molybdenum content and heat treatment on mechanical and tribological properties of a low-carbon Stellite alloy, Journal of Engineering Materials and Technology 129 (2007) 523-529.

[18] M.X. Yao, J.B.C. Wu, Y. Xie, Wear, corrosion and cracking resistance of some W- or Mo-containing Stellite hardfacing alloys, Materials Science and Engineering: A 407(1-2) (2005) 234-244.

[19] J.Y. Shen, L.X. Hu, Y. Sun, X.Y. Feng, A.W. Fang, Z.P. Wan, Hot deformation behaviors and three-dimensional processing map of a nickel-based superalloy with initial dendrite microstructure, Journal of Alloys and Compounds 822 (2020).

[20] A. Amiri, S. Bruschi, M.H. Sadeghi, P. Bariani, Investigation on hot deformation behavior of Waspaloy, Materials Science and Engineering: A 562 (2013) 77-82.

[21] R. Gujrati, C. Gupta, J.S. Jha, S. Mishra, A. Alankar, Understanding activation energy of dynamic recrystallization in Inconel 718, Materials Science and Engineering: A 744 (2019) 638-651.

[22] J. Liu, Z. Cui, L. Ruan, A new kinetics model of dynamic recrystallization for magnesium

alloy AZ31B, Materials Science and Engineering: A 529 (2011) 300-310.

[23] H.J. McQueen, S. Yue, N.D. Ryan, E. Fry, Hot Working Characteristics Of Steels In Austenitic State, Journal of Materials Processing Technology 53 (1995) 293-310.

[24] M.C. Somani, N.C. Birla, Y.V.R.K. Prasad, V. Singh, Microstructural validation of processing maps using the hot extrusion of P/M Nimonic AP-1 superalloy, Journal of Materials Processing Technology 52 (1995) 225-237.

[25] M.C. Somani, K. Muraleedharan, Y.V.R.K. Prasad, V. Singh, Mechanical processing and microstructural control in hot working of hot isostatically pressed P/M IN-100 superalloy, Materials Science and Engineering: A 245 (1998) 88-99.

[26] D. Cai, L. Xiong, W. Liu, G. Sun, M. Yao, Development of processing maps for a Ni-based superalloy, Materials Characterization 58(10) (2007) 941-946.

[27] L. Lu, L. Hou, Y. Zhang, H. Cui, J. Huang, J. Zhang, Hot Deformation Behavior and Processing Map of Spray Formed M3: 2 High Speed Steel, Journal of Iron and Steel Research International 23(5) (2016) 501-508.